

## Dynamics of Local Modes during Nonradiative Relaxation

Dana M. Calistru, S. G. Demos, and R. R. Alfano

*Institute of Ultrafast Spectroscopy and Lasers, New York State Center of Advanced Technology for Ultrafast Photonic Materials and Applications, Physics Department, The City College and Graduate School of the City University of New York, 138th Street and Convent Avenue, New York, New York 10031*

(Received 9 October 1996)

The direct participation of local modes in nonradiative processes taking place in impurity-doped laser crystals is investigated using time resolved resonance Raman scattering. The measured dynamics of the highest energy  $\text{Cr}^{4+}$  local mode in  $\text{Cr:Mg}_2\text{SiO}_4$  shows that nonradiative relaxation proceeds via transfer of the nonequilibrium local mode population generated during the transition through an electronic bottleneck, to a select number of daughter phonons, and not directly, to the phonon continuum. [S0031-9007(96)02106-0]

PACS numbers: 78.47.+p, 63.20.Kr

Understanding the role of local modes in the nonradiative relaxation is crucial to several physics areas such as laser materials, defects in dielectric crystals, and damage threshold in nonlinear crystals. Room-temperature operation of impurity-doped solid state lasers emitting in the nearinfrared and midinfrared spectral region is generally affected by nonradiative processes. The first approach to the nonradiative relaxation occurred more than four decades ago using the Born-Oppenheimer approximation which was further extended to include interactions with a spectrum of phonons [1]. Although several models were proposed to describe the nonradiative transitions in transition-metal-ion systems [2], to date there is no theory predicting the salient parameters of an impurity-doped system which may affect the energy transfer from an impurity center into the lattice environment. Studies have shown that following photoexcitation, the excess energy at the ionic site is released nonradiatively into the lattice via a limited number of distinct phonons [3,4], but no information is available on the involvement of local (impurity associated) modes in the nonradiative relaxation, although they are expected to play a crucial role in the relaxation process [5].

In this Letter, we report on the dynamics of an impurity laser ion's local modes during the nonradiative electronic-vibronic relaxation, proving the direct participation of local modes to the energy transfer from the photoexcited ion into the lattice. It is shown that the excess energy of the nonequilibrium local modes is transferred to a selected number of daughter phonons rather than, directly, to the phonon continuum. The characteristic electronic, local, and phonon modes relaxation lifetimes are obtained for the most probable decay route.

The material selected for investigation was  $\text{Cr:Mg}_2\text{SiO}_4$ , the first  $\text{Cr}^{4+}$ -based laser crystal [6].  $\text{Mg}_2\text{SiO}_4$  belongs to the olivine family and has  $Pnma$ ,  $Z = 4$  ( $D_{2h}^{16}$ ) space group symmetry, with lattice constants  $a = 10.22 \text{ \AA}$ ,  $b = 5.99 \text{ \AA}$ , and  $c = 4.76 \text{ \AA}$ .  $\text{Cr}^{4+}$  substitutes for  $\text{Si}^{4+}$  in a tetrahedrally distorted position with  $C_s$  site symmetry (which is sometimes approximated

by  $C_{2v}$  [7]). The sample was a  $10 \times 8 \times 6 \text{ mm}^3$  oriented  $\text{Cr:Mg}_2\text{SiO}_4$  single crystal. All measurements were performed at room temperature.

$\text{Cr}^{4+}$  ions were excited near the zero-phonon line of the  ${}^3B_2({}^3T_1)$  state [7] with linearly polarized 598 nm excitation, corresponding to the maximum anti-Stokes resonance enhancement for the highest frequency, highest scattering cross section  $765 \text{ cm}^{-1}$   $\text{Cr}^{4+}$  local mode [8]. 500 fs, 598 nm excitation pulses were obtained by synchronously pumping a Rh-6G dye laser with a mode-locked Nd:YAG laser (82 MHz repetition rate) whose output pulses were compressed by a pulse compressor (before entering the dye laser) to  $\sim 4$  ps (at 532 nm). The  $\sim 40$  mW excitation pulse measured at the sample site was split into pump and probe pulses with intensity ratio 2/1, respectively. The spectral pulse width was  $\sim 35 \text{ cm}^{-1}$ . The probe pulse entered an adjustable time-delay unit where it was retarded by a variable time  $\Delta t$  with respect to the pump pulse. The probe pulse was then recombined with the pump pulse and focused into the sample to an estimated  $20 \mu\text{m}$  diameter spot, in a back-scattering geometry using a microscope objective.

Polarized anti-Stokes spectra corresponding to totally symmetric  $A_g$  modes were collected for different time delays  $\Delta t$  using a SPEX triple spectrometer with spectral resolution  $5 \text{ cm}^{-1}$  and a PIAS, Hamamatsu C1815 photon counter. The change in the intensity of the  $765 \text{ cm}^{-1}$   $\text{Cr}^{4+}$  local mode, indicating the transient presence of nonequilibrium local mode population following photoexcitation of  $\text{Cr}^{4+}$  ions was monitored. The 609 and 826–856  $\text{cm}^{-1}$  phonon modes were selected as reference since they are not involved in the nonradiative relaxation process [4]. In addition, the dynamics of the  $335 \text{ cm}^{-1}$  daughter phonon modes involved in the most probable decay pathway of the  $765 \text{ cm}^{-1}$  local mode was investigated.

Figure 1 displays the measured anti-Stokes  $A_g$  spectra, in the  $500\text{--}900 \text{ cm}^{-1}$  spectral range, under the above described experimental conditions, at two different time delays following photoexcitation: (a)  $\Delta t = 3$  ps, continuous-line profile, and (b)  $\Delta t = 35$  ps, dashed-line

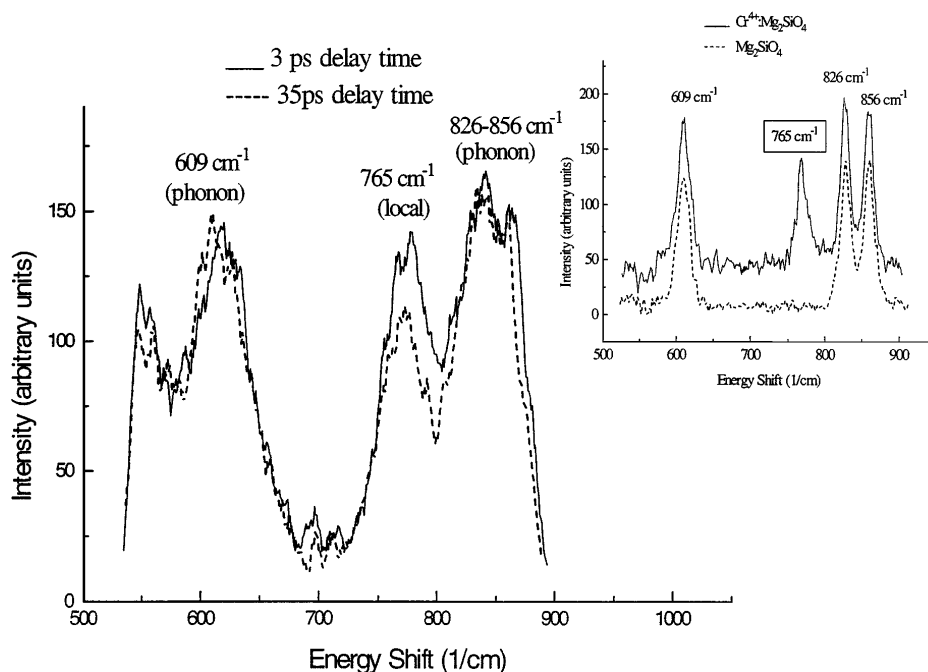


FIG. 1. Time resolved  $\text{Cr}:\text{MgSiO}_4$  anti-Stokes  $A_g$  spectra obtained at room temperature under 598 nm excitation wavelength, for (a)  $\Delta t = 3$  ps and (b)  $\Delta t = 35$  ps pump-probe delay time, in the 500–900  $\text{cm}^{-1}$  spectral region. The inset shows anti-Stokes resonance Raman (continuous line) and Raman (dashed line)  $A_g$  spectra, for  $\text{Cr}^{4+}:\text{MgSiO}_4$  and  $\text{Mg}_2\text{SiO}_4$ , respectively, obtained under 598 nm excitation wavelength, in the 500–900 nm spectral range.

profile. The increased intensity of the  $765\text{ cm}^{-1}$  local mode 3 ps after photoexcitation indicates the transient presence of nonequilibrium local mode population. The inset in Fig. 1 presents anti-Stokes resonance Raman (continuous line) and Raman (dashed line)  $A_g$  spectra, for  $\text{Cr}^{4+}:\text{MgSiO}_4$  and  $\text{Mg}_2\text{SiO}_4$ , respectively, obtained under 598 nm excitation, in the 500–900 nm spectral range. The  $765\text{ cm}^{-1}$   $\text{Cr}^{4+}$  local mode is boxed. The spectral pulse width was  $\sim 5\text{ cm}^{-1}$  for both spectra shown in the inset.

The normalized relative change in the integrated (over  $26\text{ cm}^{-1}$ ) intensity of the  $765\text{ cm}^{-1}$  local mode, taking as reference the  $609\text{ cm}^{-1}$  integrated (over  $26\text{ cm}^{-1}$ ) constant phonon mode intensity, for different time delays  $\Delta t$  is shown in Fig. 2 (filled boxes). The measured dynamics of the  $335\text{ cm}^{-1}$  daughter phonon mode is also depicted in Fig. 2 (open circles). The temporal profiles presented in Fig. 2 demonstrate that the nonequilibrium local mode population builds up during the initial 3–4 ps following photoexcitation, while the nonequilibrium phonon mode population reaches its maximum  $\sim 8$  ps following photoexcitation.

To explain the experimental data and estimate the characteristic lifetimes of the subsystems involved in the nonradiative decay process, the following model, schematically depicted in Fig. 3, was developed. The 598 nm pump pulse photoexcites  $\text{Cr}^{4+}$  ions near the zero-phonon line of the  ${}^3B_2({}^3T_1)$  state, creating an excited state population  $\eta(t)$ . The lack of emission from the  ${}^3B_2({}^3T_1)$  state suggests that  $\text{Cr}^{4+}$  ions relax nonradiatively towards the metastable level at 9150 nm,

by making a transition to the lower lying  ${}^1E$  state. As the above-mentioned transition is spin forbidden, the system requires a longer tunneling time  $\Gamma^{-1}$ , giving rise to an electronic bottleneck ( $\Gamma$  is the transition rate probability of the system through the electronic bottleneck). The presence of the  ${}^3B_2({}^3T_1)\text{-}{}^1E$  bottleneck was first reported using the up-converted hot luminescence technique, and its lifetime was measured to

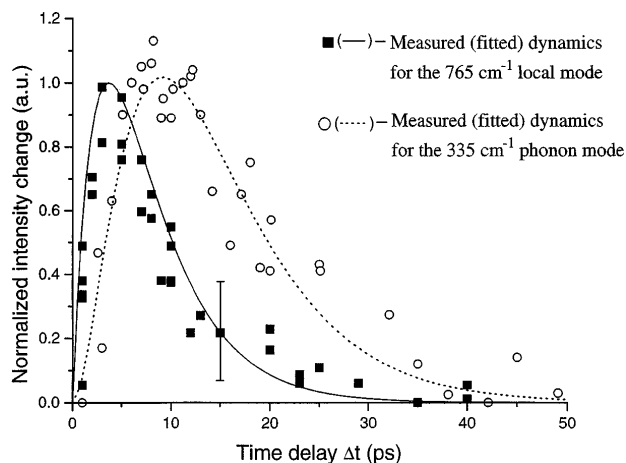


FIG. 2. Normalized measured ( $\blacksquare, \circ$ ) and fitted (—, - - -) dynamics for the  $765\text{ cm}^{-1}$  (local) and  $335\text{ cm}^{-1}$  (phonon) modes, respectively. Best fits were obtained using the following parameters from the intermolecular relaxation pathway: electronic bottleneck transition time  $\Gamma^{-1} = 2.8$  ps, local mode lifetime  $g_1^{-1} = 5.1$  ps, and phonon mode lifetime  $g_{30}^{-1} = 5$  ps.

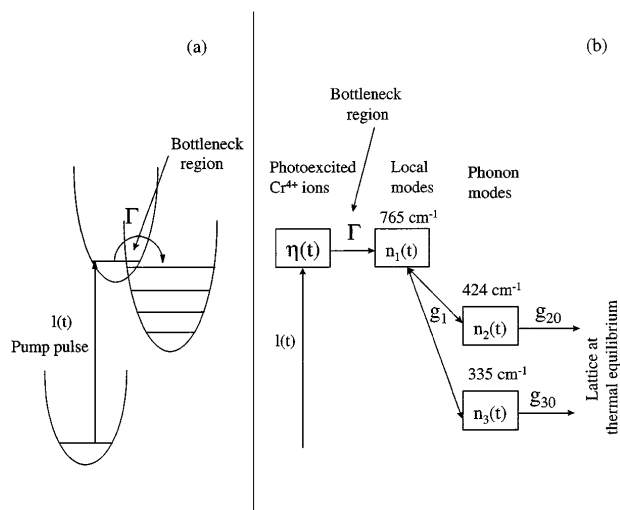


FIG. 3. (a) Schematic diagram showing the increase in the local mode population following the crossing of the  ${}^3B_2({}^3T_1)\text{-}{}^1E$  electronic bottleneck; (b) intermolecular nonradiative relaxation pathway for the  $765 \text{ cm}^{-1}$  local mode and characteristic decay rates.

be  $\Gamma^{-1} < 10 \text{ ps}$  [9]. It was also shown that the next lower lying  $\text{Cr}^{4+}$  bottleneck, with an estimated lifetime of the order of hundreds of nanoseconds, appears at  $\sim 735 \text{ nm}$  [bottom of  ${}^3A_2({}^3T_1)$  state] [10]. As the electronic transition is accompanied by an increase in the occupation number for local modes [electronic-vibronic transitions, see Fig. 3(a)], it is expected that the nonequilibrium local mode population rises during the time needed to cross the electronic bottleneck,  $\Gamma^{-1}$ .

Following the transition through the electronic bottleneck, the local mode population decays nonradiatively. The energy of the nonequilibrium local mode population can be transferred nonradiatively into the lattice by one of the following processes: The local mode interacts with the lattice represented by a continuum of phonon modes and distributes the excess energy into the reservoir (discrete-to-continuum energy transfer), and/or the local mode interacts with a very restricted number of vibrations (daughters) which take over the excess energy and display a transient, "time-shifted" (from the driving local mode) nonequilibrium population (discrete-to-discrete energy transfer). The most likely energetic-wise daughter decay channels for the investigated  $765 \text{ cm}^{-1}$  local mode are (a) decay into two phonon modes  $\omega_{1P} + \omega_{2P}$  (intermolecular decay), such that  $765 \text{ cm}^{-1} \rightarrow \omega_{1P} + \omega_{2P}$  with  $\omega_{1P} = 335 \text{ cm}^{-1}$  and  $\omega_{2P} = 424 \text{ cm}^{-1}$ ; or (b) decay into two local modes  $\omega_{1L} + \omega_{2L}$  (intramolecular decay), such that  $765 \text{ cm}^{-1} \rightarrow \omega_{1L} + \omega_{2L}$  with  $\omega_{1L} = 346 \text{ cm}^{-1}$  and  $\omega_{2L} = 420 \text{ cm}^{-1}$ . The nonequilibrium local mode population transfers into nonequilibrium phonon mode population [for both cases (a) and (b)]. As the nonequilibrium mother local mode population decreases, the nonequilibrium daughter phonon modes which are driven by this particular decay route increase. The nonequilibrium daughter phonon mode

population decays by interactions with the phonon continuum allowing the system to return to thermal equilibrium.

It should be mentioned that the inset in Fig. 1 shows that there are no phonon or local modes in resonance with the  $765 \text{ cm}^{-1}$  local mode, indicating that resonance nonradiative processes cannot occur for this local mode. Discrete-to-discrete energy decay pathways were first investigated in liquids [11] where it was shown that intermolecular resonance processes are possible [12].

The temporal profiles in Fig. 2 show that the  $335 \text{ cm}^{-1}$  daughter phonon is created during the decay of the  $765 \text{ cm}^{-1}$  local mode, indicating a discrete-to-discrete pathway. It should be noted that no information can be obtained on the dynamics of the  $424 \text{ cm}^{-1}$  daughter phonon mode which is too weak to be resolved in an anti-Stokes Raman spectrum.

Group symmetry selection rules show that the intermolecular decay pathway case (a) is allowed but the intramolecular pathway case (b) is not [13]. The relevant modes of vibration for the  $765 \text{ cm}^{-1}$  decay pathway have the following symmetries: the  $765$  and  $346 \text{ cm}^{-1}$  local [14] and  $335$  and  $424 \text{ cm}^{-1}$  phonon modes [15] appear in  $A_g$  spectra, i.e., are totally symmetric in  $C_s$  ( $A'$ ). The  $420 \text{ cm}^{-1}$  local mode is nontotally symmetric in  $C_s$  ( $A''$ ) [14]. The intermolecular decay pathway [case (a)] involves three totally symmetric vibrations:  $765$ ,  $335$ , and  $424 \text{ cm}^{-1}$ . As the product of the three  $A'$  wave functions is  ${}^{13}A' \times A' \times A' = A'$ , i.e., totally symmetric, the intermolecular decay pathway is allowed. On the other hand, the intramolecular decay pathway [case (b)] involves two  $A'$  local modes ( $765$  and  $346 \text{ cm}^{-1}$ ) and one nontotally symmetric  $A''$  local mode ( $420 \text{ cm}^{-1}$ ) [14]. As the product of these three wave functions is  ${}^{13}A' \times A' \times A'' = A''$ , i.e., nontotally symmetric, the intramolecular decay pathway is forbidden.

The intermolecular nonradiative decay pathway can be modeled using the scheme depicted in Fig. 3(b). The equations describing the dynamics of the ion-lattice system can be solved exactly for a  $\delta$ -shaped laser pulse. The best fit was obtained for the following characteristic parameters, schematically depicted in Fig. 3(b): bottleneck transition time  $\Gamma^{-1} = 2.8 \pm 0.3 \text{ ps}$ , local mode lifetime  $g_1^{-1} = 5.1 \pm 0.5 \text{ ps}$ , phonon mode lifetime  $g_{30}^{-1} = 5 \pm 0.5 \text{ ps}$ . Figure 2 shows the calculated dynamics for the  $765 \text{ cm}^{-1}$  local (continuous line) and  $335 \text{ cm}^{-1}$  daughter phonon (dotted line) modes using the above-mentioned parameters. All fits were performed using a nonlinear least-squares fit. More realistic laser pulse shapes do not lead to significant changes in these characteristic relaxation lifetimes. It should be noted that the lack of information on the dynamics of the  $424 \text{ cm}^{-1}$  phonon mode does not affect the determination of the characteristic lifetimes, as  $\Gamma^{-1}$  and  $g_1^{-1}$  (local mode lifetime) are given by the dynamics of the  $765 \text{ cm}^{-1}$  local mode (which was measured), and the daughter phonon lifetimes ( $g_{20}^{-1}$  and  $g_{30}^{-1}$ ) are independent.

In conclusion, we have measured the dynamics of local and phonon modes during the electronic-vibronic non-radiative relaxation of a photoexcited laser impurity ion proving the active participation of local modes in the non-radiative relaxation process. We have shown that the nonequilibrium local mode population builds up during the transition through an electronic bottleneck and decays by interaction with a restricted number of phonon modes (discrete-to-discrete energy transfer) rather than through direct interaction with the phonon continuum. This leads to a time-shifted temporal profile for the nonequilibrium daughter phonons with respect to the dynamics of the nonequilibrium mother local mode (Fig. 2) such that the daughters peak at  $\sim\Gamma^{-1} + g_1^{-1} \approx 8$  ps. The following key parameters were determined for the system under investigation ( $\text{Cr}^{4+}$  in  $\text{Cr:Mg}_2\text{SiO}_4 : {}^3B_2({}^3T_1) \rightarrow {}^1E$  electronic bottleneck transition time  $2.8 \pm 0.3$  ps, local mode lifetime (due only to an intermolecular anharmonic decay channel)  $5.1 \pm 0.5$  ps, birth time of daughter phonons  $7.9 \pm 0.6$  ps, and lifetime of daughter phonons (due to interaction with the continuum of phonons)  $5 \pm 0.5$  ps.

We thank Dr. R. Guenther and Dr. M. Ciftan for their continued support for this research. This work was supported in part by the Army Research Office.

- 
- [1] M. Lax, *J. Chem. Phys.* **20**, 1752 (1952).  
 [2] R.H. Bartram, J.C. Charpie, L.J. Andrews, and A. Lempicki, *Phys. Rev. B* **34**, 2741 (1986).  
 [3] S.G. Demos, J.M. Buchert, and R.R. Alfano, *Appl. Phys. Lett.* **61**, 660 (1992).  
 [4] S.G. Demos and R.R. Alfano, *Phys. Rev. B* **52**, 987 (1995).  
 [5] R. Englman, *Non-Radiative Decay of Ions and Molecules in Solids* (North-Holland Publishing Co., Amsterdam, 1979).  
 [6] V. Petricevic, S.K. Gayen, and R.R. Alfano, *Appl. Phys. Lett.* **53**, 2590 (1988).  
 [7] W. Jia, H. Liu, S. Jaffe, W. M. Yen, and B. Denker, *Phys. Rev. B* **43**, 5234 (1991).  
 [8] Dana M. Calistru, W.B. Wang, V. Petricevic, and R.R. Alfano, *Phys. Rev. B* **51**, 14980 (1995).  
 [9] S.G. Demos, Y. Takiguchi, and R.R. Alfano, *Opt. Lett.* **18**, 522 (1993).  
 [10] S.G. Demos, V. Petricevic, and R.R. Alfano, *Phys. Rev. B* **52**, 1544 (1995).  
 [11] R.R. Alfano and S.L. Shapiro, *Phys. Rev. Lett.* **29**, 1655 (1972).  
 [12] A. Laubereau, G. Kehl, and W. Kaiser, *Opt. Commun.* **11**, 74 (1974).  
 [13] A certain phonon decay pathway is allowed if the product of the wave functions of the vibrational modes involved in this particular route is equal to or contains the totally symmetric representation (i.e., the representation which is invariant under all the operations of the group) [16]. The group describing the symmetry of different phonon and local modes is the site symmetry. On the other hand, the experimental results are obtained in terms of the symmetry of the unit cell (space group symmetry). The information provided by the symmetry of the unit cell can be reduced to results describing the site symmetry by making use of correlation tables [17]. Correlation tables for the site ( $C_s$ ) and space group ( $D_{2h}$ ) symmetries for a  $\text{Cr:Mg}_2\text{SiO}_4$  system show that *all* totally symmetric  $D_{2h}$  modes ( $A_g$ ) originate *only* from totally symmetric  $C_s$  modes ( $A'$ ). The simple structure of a  $C_s$  group (which contains only one plane of reflection) leads to two representations:  $A'$  (totally symmetric) and  $A''$  (nontotally symmetric), with the following multiplication laws:  $A' \times A' = A'$ ,  $A' \times A'' = A'' \times A' = A''$ , and  $A'' \times A'' = A'$ .  
 [14] Dana M. Calistru, S.G. Demos, and R.R. Alfano, *Phys. Rev. B* **52**, 15253 (1995).  
 [15] K. Iishi, *Am. Mineral.* **63**, 1198 (1978).  
 [16] Joseph L. Birman, *Theory of Crystal Space Groups and Lattice Dynamics* (Springer-Verlag, Berlin, 1984).  
 [17] W.G. Fateley, F.R. Dolish, N.T. McDevitt, and F.F. Bentley, *Infrared and Raman Selection Rules for Molecular and Lattice Vibrations* (Wiley Interscience, New York, 1972).